

RESEARCH ARTICLE

Forecasting the path of a laterally propagating dike

10.1002/2015JB012402

Key Points:

- Model for forecasting lateral dike intrusions is presented
- Hindcasts are shown to agree well with observed paths of two dikes
- Topography can strongly influence a dike path

Correspondence to:

E. R. Heimisson,
eliasrh@stanford.edu

Citation:

Heimisson, E. R., A. Hooper, and F. Sigmundsson (2015), Forecasting the path of a laterally propagating dike, *J. Geophys. Res. Solid Earth*, 120, 8774–8792, doi:10.1002/2015JB012402.

Received 28 JUL 2015

Accepted 3 DEC 2015

Accepted article online 12 DEC 2015

Published online 28 DEC 2015

Elías Rafn Heimisson^{1,2}, Andrew Hooper³, and Freysteinn Sigmundsson¹

¹Nordic Volcanological Center, Institute of Earth Sciences, University of Iceland, Reykjavik, Iceland, ²Department of Geophysics, Stanford University, Stanford, California, USA, ³Centre for the Observation and Modelling of Earthquakes and Tectonics (COMET), School of Earth and Environment, University of Leeds, Leeds, UK

Abstract An important aspect of eruption forecasting is predicting the path of propagating dikes. We show how lateral dike propagation can be forecast using the minimum potential energy principle. We compare theory to observed propagation paths of dikes originating at the Bárðarbunga volcano, Iceland, in 2014 and 1996, by developing a probability distribution for the most likely propagation path. The observed propagation paths agree well with the model prediction. We find that topography is very important for the model, and our preferred forecasting model considers its influence on the potential energy change of the crust and magma. We tested the influence of topography by running the model assuming no topography and found that the path of the 2014 dike could not be hindcasted. The results suggest that lateral dike propagation is governed not only by deviatoric stresses but also by pressure gradients and gravitational potential energy. Furthermore, the model predicts the formation of curved dikes around cone-shaped structures without the assumption of a local deviatoric stress field. We suggest that a likely eruption site for a laterally propagating dike is in topographic lows. The method presented here is simple and computationally feasible. Our results indicate that this kind of a model can be applied to mitigate volcanic hazards in regions where the tectonic setting promotes formation of laterally propagating vertical intrusive sheets.

1. Introduction

Physically complete and realistic numerical models of dike propagation have not yet been developed. This is due to the complexity and computational impracticality of considering all factors that may affect dike propagation [Rivalta *et al.*, 2015]. The aim of this study is to present a simple and fast approach for forecasting the path of a laterally propagating dike. In earth science, simplifying assumptions are required due to the Earth's heterogeneous nature, the details of which are unknown. A forecasting model of any sort should consider such simplifications and assumptions, as well as propagate errors of the input parameters whenever possible. For complex and computationally expensive numerical models, such error propagation might be difficult on the time scale in which dikes propagate and when results are required as soon as possible.

To achieve this goal we present an approach that is able to hindcast the path of the 2014 and 1996 intrusions originating at the Bárðarbunga volcano, Iceland [Sigmundsson *et al.*, 2015; Einarsson *et al.*, 1997]. The 2014 dike intrusion is well documented and demonstrates segmented propagation with significant changes in strike. A dike's direction of propagation is influenced by the orientation of the least compressive stress (σ_3) [Anderson, 1951]. However, it has been shown that other factors (e.g., dike driving pressure, structural, elastic, and/or density discontinuities) may favor different opening directions. Moreover, measuring deviatoric stresses in the crust is difficult, and verifying with observations whether a dike propagates exactly perpendicular to σ_3 is thus challenging. The Bárðarbunga 2014 intrusion showed that dike emplacement was not completely perpendicular to the least compressive stress. This was seen in modeling of geodetic data, as significant strike-slip motion accompanied dike formation [Sigmundsson *et al.*, 2015, supplementary Figure 4]. Few lateral diking events have been monitored with such high accuracy in hypocentral locations and geodetic measurements as the 2014 Bárðarbunga dike, where relative errors of relocated hypocenters are generally less than 200 m in longitude and latitude, thus providing excellent constraints on models of geodetic data. Modeling of the Upptyppingar 2007–2008 dike in Iceland also demonstrated that geodetic data could not be explained without a shear displacement along the plane of the dike [Hooper *et al.*, 2011]. This strongly suggests that emplacement is not perpendicular to σ_3 . While it is evident that orientation of the principal stresses plays an important role in determining dike propagation orientation, the cases of the 2014 Bárðarbunga dike and Upptyppingar 2007–2008 dike confirm that other factors should also be considered.

Several studies have found that factors other than deviatoric stresses can influence dike formation. *Pollard and Muller* [1976] found that a gradient in magma pressure or lithostatic pressure was a plausible explanation for the tear-drop shape some dikes show in horizontal cross section. This indicates that the equilibrium configuration of the crust after a dike intrusion, where the total potential of an elastic body is at a minimum [Reddy, 2013], is influenced by pressure gradients. *Dahm* [2000] concluded that the tectonic stress gradient, length of fractures, and buoyancy all influenced the orientation of vertically propagating magma. *Watanabe et al.* [2002] demonstrated, using analog experiments, that there is an interplay between dike driving pressure and directions of principal stress. *Mériaux and Lister* [2002] concluded that the dike alters the stress field as it propagates and, therefore, does not follow the principal stress trajectories in the crust before the diking event. The study by *Sigmundsson et al.* [2015] showed that a dike propagation model that considered strain and gravitational energy changes due to topography could well explain the observed changes in strike. Here we explore further the role of topography and how the fact that it is easily measurable can help us to forecast lateral dike propagation with reasonable accuracy when we also have a reasonable model of the plate motion strain.

A propagating dike tip can be expected to be emplaced in such a way that the total potential of the system is at a minimum. The minimum potential energy principle is a far-reaching variational principle [Reddy, 2013]. One can equivalently state that the emplacement should be such that it allows for the greatest energy release. This can be interpreted as the path of least resistance. We apply it here to quasi-static dike propagation, which means we do not consider the details of the magma flow within the dike. Similar methods have been used successfully in studying dike propagation [e.g., *Dahm*, 2000; *Maccaferri et al.*, 2011, 2014]. We introduce several new aspects to this approach, including pressure changes due to realistic topography.

The total potential energy function U_T can be written as a sum of the relevant terms

$$U_T = \Theta_s + \Phi_g \quad (1)$$

where $\Theta_s = \theta_c + \theta_f$, i.e., the sum of the strain energy of the crust and of the fluid inside the crack, respectively, and $\Phi_g = \phi_c + \phi_f$ is composed of the gravitational energy of the crust and the gravitational energy of the fluid inside the crack, respectively. When an isolated blob of magma propagates, such as was studied by *Dahm* [2000] and *Maccaferri et al.* [2011] we expect all these terms to contribute the total potential and influence the dike propagation in a straightforward manner. However, a laterally propagating dike, as is studied here, is only a part of a more complicated system, i.e., a system of a coupled magma chamber, the crust and a dike. Due to the difficulty of knowing the details of a magma chamber a priori, we only look at the dike, whose position, depth, and geometry can all be constrained relatively well with seismic and geodetic data. However, the energy released due to deflation of a magma chamber is proportional to the volume that is released and is thus proportional to the dike tip opening. We can therefore infer how including it in a model might influence the results. See further discussion of this effect and other considerations of the energy changes of the more complicated system in section 4.4.

In our model, the dike tip is a vertical, laterally propagating crack where the upper and lower margins are at fixed depth with respect to the elevation of the topography. Because the Bárðarbunga volcano and surroundings are covered by an ice cap with a thickness of about a few hundred meters, we essentially have two topographic surfaces, of the ice and bedrock. We reference the depth to a single surface by taking the ice thickness and multiplying by the ratio of the density of the ice and bedrock and then add to the elevation of the bedrock topography.

The path of the dike is systematically lengthening as the crack tip is emplaced in such a way that it minimizes the potential energy. In the following we will consider the change in the potential ΔU_T rather than its absolute value when evaluating different propagation directions. We determine the propagation path that causes the greatest energy release or, in other words, the greatest lowering of the potential energy, so evaluating the absolute potential energy is not necessary. We have assumed that the magma is incompressible, so the strain energy change of the magma is zero ($\Delta\theta_f = 0$), which is one of the four terms initially presented in equation (1). This assumption is reasonable because we consider a laterally propagating dike tip that is propagating at the level of neutral buoyancy (LNB) and thus not exposed to significant changes in confining pressure.

The approach we present here allows us to create a probability density function (PDF) for dike propagation paths in near-real time without requiring great computational power. All computations presented in this

paper were carried out on a regular laptop. Although the method presented by *Sigmundsson et al.* [2015] could have been implemented for a similar purpose, it was too computationally expensive to be used for building a distribution of the most likely path of the dike in near-real time. We estimate the approach presented here to be on the order of 1000 times faster than that of *Sigmundsson et al.* [2015]. In *Sigmundsson et al.* [2015], the dike was assumed to propagate at a fixed depth with respect to sea level. Here we look at a dike propagating at the LNB and is thus at fixed depth below the topography. LNB propagation has been proposed as a likely explanation for lateral flow of magma in dikes [e.g., *Lister and Kerr*, 1991; *Fiske and Jackson*, 1972; *Fialko and Rubin*, 1999] and is thus perhaps more realistic than fixed-depth propagation. Furthermore, the depth changes in seismicity and changes in lithostatic pressure were found to be correlated for the Bárðarbunga 2014 dike, suggesting LNB propagation [*Heimisson*, 2015]. The dike is assumed to propagate at 2.5 km below the topographic elevation, having a width (height) of 5 km. This is in broad agreement with estimates from the geodetic modeling of the 2014 Bárðarbunga dike [*Sigmundsson et al.*, 2015]. We presented a method to evaluate the gravitational energy change due to topography in *Sigmundsson et al.* [2015] that assumed the topography to be point masses distributed on the surface of a half-space. Here we apply a different method, which allows us to relax many of the assumptions behind that model, such as fixed depth propagation. The crack model presented by *Sigmundsson et al.* [2015] to evaluate the propagation path assumed the opening to be constant, and the crack tip was composed of only one rectangular dislocation. Assuming constant opening, which is independent of strike, requires information about the actual dike opening, which is difficult to attain without first modeling geodetic displacement. Here the crack tip is a single column of 10 rectangular dislocations and is generally shorter in the along-strike direction. In *Sigmundsson et al.* [2015], we required ad hoc measures to avoid stress singularities in a volumetric strain energy integral, which may have led to inaccurate integral evaluations. Based on *Dahm* [2000], we use a boundary element method (BEM) coupled with evaluating the energy change of the crust as a surface integral to resolve these issues of the volumetric strain integral. The BEM allows us to solve for opening of the dike tip. This resolves the aforementioned problems of assuming constant opening independent of strike. Furthermore, we expand on the work by *Maccaferri et al.* [2011], which looked at vertical migration of magma with constant mass in two dimensions. We extend their formulation into three dimensions, which allows us to study laterally propagating dikes. For the sake of simplicity and computational efficiency, however, we do not model changes in the vertical extent of the dike. We also compare our results to actual observations of dike propagation and show that the topography has a large influence on the propagation path. Our results show that even though a large uncertainty affects the model of the stress field, the influence of the topography is so great that a dike propagation path can be constrained with relatively good accuracy and therefore that near-real-time prediction of the propagation path of laterally propagating dikes is possible.

2. Propagation Model

2.1. Energy Change of the Crust

The energy change $\Delta\theta_c + \Delta\phi_c$ due to slip on surface Σ is given by equation (2) [*Dahlen*, 1977; *Savage and Walsh*, 1978]. Note that this equation accounts for not only the strain energy change, as is often stated, but also the total energy change of the crust (see section 4.2 for a detailed explanation of this issue). One side of the surface is Σ^- and the other one Σ^+ . \mathbf{v} is the normal to Σ . The displacement is described by $[\mathbf{u}]$, which is the difference between displacements on Σ^+ and Σ^- . We have

$$\Delta\theta_c + \Delta\phi_c = -\frac{1}{2} \int_{\Sigma} [u_i] \left(\sigma_{ij}^0 + \sigma_{ij}^1 \right) v_j d\Sigma \quad (2)$$

where σ_{ij}^0 is the stress tensor acting at a point on Σ before slip and/or opening and σ_{ij}^1 after slip and/or opening.

To evaluate the energy change from crack opening, we need the absolute stress field. From the stress field, we can calculate traction on a crack surface. Once the crack is opened and filled with low-viscosity fluid, the shear traction will vanish; however, the normal component of the traction vector does not. From these changes in traction we can calculate the displacements of the crack surface using a BEM. Once the displacements are estimated, we can calculate the energy change of the crust.

In the following, we adapt the methodology described by *Maccaferri et al.* [2011] to three dimensions to evaluate this integral. The crack surface is discretized into rectangular patches, each assumed to have

uniform stress change on the surface. We can write the stress before slip as the sum of the following terms on one patch:

$$\sigma_{ij}^0 = P_{\text{litho}}\delta_{ij} + \sigma_{ij}^T \quad (3)$$

where P_{litho} is the lithostatic pressure, δ_{ij} the Kronecker delta, and σ_{ij}^T the stress contribution of plate motion or other causes that contribute to stresses in the crust other than pressure. Lithostatic pressure is calculated assuming the density model for the crust described in Appendix A.

It is more convenient for the BEM if equation (3) is written in terms of components of the traction vector in the basis of the unit normal v_i , the dip vector v_i^d , and the strike vector v_i^s of each point of the crack:

$$\text{Normal: } T_n^0 = \sigma_{ij}^0 v_j v_i \quad \text{Dip: } T_d^0 = \sigma_{ij}^0 v_j v_i^d \quad \text{Shear: } T_s^0 = \sigma_{ij}^0 v_j v_i^s \quad (4)$$

The traction vector in the basis of these orthogonal vectors before crack opening is thus

$$\mathbf{T}^0 = (T_n^0, T_d^0, T_s^0) \quad (5)$$

The traction vector after crack opening is

$$\mathbf{T}^1 = (T_n^0 - \Delta P, 0, 0) \quad (6)$$

Once a crack opens and is filled with low-viscosity fluid, all shear terms will become zero. ΔP is the difference between the fluid pressure and the confining pressure:

$$\Delta P = P_{\text{fluid}} - P_{\text{conf}} \quad (7)$$

The fluid pressure can be written as

$$P_{\text{fluid}} = \rho_f g(z_T - z) + P_{\text{ex}} + P_{\text{litho}}^1 \quad (8)$$

where ρ_f is the density of the magma, z is the vertical location of the patch, and z_T is the top rim of the dike at the starting point of propagation. The term $\rho_f g(z_T - z)$ thus represents the hydrostatic pressure inside the dike tip. The z axis is considered positive upward. P_{ex} is extra pressure which may be caused by a connection to a pressurized magma reservoir and may decay as the dike propagates. P_{litho}^1 is the lithostatic pressure at the top rim of the dike where it first opens and begins to propagate. Where the dike first opens, it must have fluid pressure equal to the effective normal stress on the crack surface plus overpressure to fracture the rock. However, it is unrealistic to change the assumed fluid pressure depending on the strike of the segment. We, therefore, use the lithostatic pressure in equation (8) to estimate the fluid pressure. The dike is therefore guaranteed to have nonnegative opening in any direction because, at a divergent plate boundary the lithostatic pressure functions as an upper limit to the effective normal stress. The assumed magma pressure will consequently not be a function of strike. The confining pressure, however, should be a function of the strike, and we account for that in equation (9). Determining the extra pressure P_{ex} is difficult. Some studies might suggest that extra pressure would be needed to fracture the rock and should account for the tensile strength of the host rock. *Schultz* [1995] estimated an intact block of basalt at room temperature to have tensile strength of 14.5 ± 3.3 MPa. This value would suggest that considerable extra pressure would be needed. However, *Jónsson*, 2012] studied kilometer-scale tensile strength of granite and found it to be up to an order of magnitude less than the typical laboratory values, which suggests that a much lower extra pressure, if any, is needed for propagation. For the final model runs presented in the results we set $P_{\text{ex}} = 0$. We found that relatively small values of the extra pressure in the range 0–5 MPa did not have significant influence on the results; however, larger values cause unrealistic behavior as is discussed further in section 4.3. Because the dike tends to propagate downhill, the hydrostatic pressure increases in the tip. This effect causes inflation of the dike tip in topographic lows (Figure 1). Even though the lithostatic pressure is constant in LNB propagation, the fluid pressure and overpressure is generally increasing.

The confining pressure is

$$P_{\text{conf}} = P_{\text{litho}}(z) + \sigma_{ij}^T v_i v_j \quad (9)$$

where $\sigma_{ij}^T v_i v_j$ is the component of stress other than pressure that is normal to Σ . Note that the normal traction on Σ after opening of the dike is just the magma pressure at that depth. We calculate ΔP according to

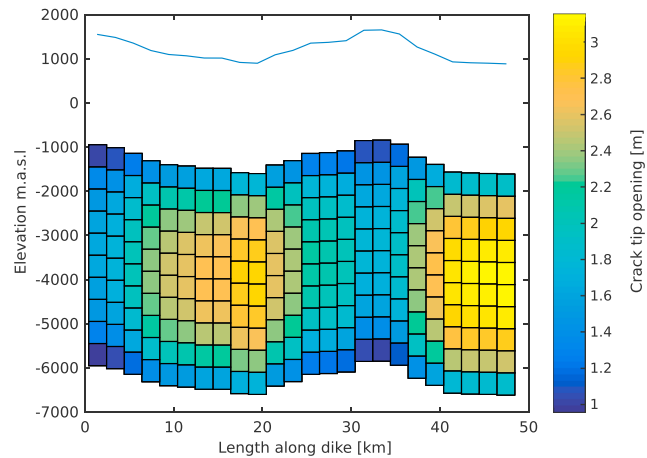


Figure 1. Example of how the dike tip opening changes depending on the topography. In this example simulation, the dike path was constrained to go along a straight line to make the figure simpler. The blue line above shows the bedrock topography. Notice how low topography correlates with large opening. This is because the magma pressure is increased in topographic lows.

equation (7), however, because $-\Delta P$ is the change to the normal traction before and after opening and it is the quantity we require to solve for opening in the BEM.

Now, equation (2) can be replaced by a sum over k patches:

$$\Delta\theta_c + \Delta\phi_c \approx -\frac{1}{2} \sum_{l=1}^k \left[b'_n (T_n^{0,l} + T_n^{1,l}) + b'_d T_d^{0,l} + b'_s T_s^{0,l} \right] \Sigma^l \quad (10)$$

where l is the number of a patch and Σ^l is the area of patch number l . $T_i^{0,l} + T_i^{1,l}$ are the i th component of the traction vector acting on patch number l , where 0 indicates the traction vector before opening and 1 indicates the traction vector after opening.

The components of the vector $\mathbf{b}' = (b'_o, b'_d, b'_s)$ represent opening, slip in the strike direction, and slip in the dip direction at patch number l , respectively. In LNB propagation, the fluid pressure (equation (8)) is a function of the elevation of the topography. It therefore influences the overpressure of the dike tip (equation (7)), which in turn, changes the normal traction after opening in equation (10). The energy change of the crust thus becomes a function of the elevation of the topography. We find that this hydrostatic pressure gradient induced by the topography is very important because it heavily influences how much strain energy can be released during the dike emplacement. Note that if the dike does not follow LNB, equation (9) also becomes a function of the elevation of the topography because the dike will be exposed to changes in confining pressure.

2.2. Gravitational Potential Change of the Magma

The gravitational potential of the magma in a dike tip can be written:

$$\phi_f = \rho_f V g Z^1 \quad (11)$$

where Z^1 is the z component of the center of mass of the magma in the tip and V is the volume of the tip. To get the change in potential energy, we must consider where the magma is being supplied. Assuming that it being transported laterally from the starting point of the first segment of the dike, we can express the difference in gravitational energy change of the magma:

$$\Delta\phi_f = V \rho_f g (Z^1 - Z^0) \quad (12)$$

where Z^0 is the center of mass of the first segment. Note that if the dike is always traveling at a fixed depth with respect to sea level, this model predicts no change in gravitational energy of the magma, as would be expected.

If we consider a LNB propagation laterally away from a cone, the dike begins by traveling downhill, but once outside the cone, it will move at fixed depth with respect to the z axis. At first glance one might think that

the magma would, at that point, have no change in gravitational energy. This is not the case, however, as the initial downhill emplacement of the dike results in magma flowing downhill when new segments are added to the end. This favors the crack orientation that allows for the greatest opening, because that results in the largest downhill mass transfer. This is also the orientation that is perpendicular to σ_3 .

We assume that the magma has a density $\rho_f = 2700 \text{ kg/m}^3$, which is the same as the average density for the layer in which the dike is assumed to propagate (see Appendix A). The criteria for LNB propagation is therefore met.

2.3. Plate Boundary Stress Model

Our model is highly dependent on the state of stress in the crust. One of the major causes for deviatoric stress accumulation at plate boundaries is motion of the tectonic plates. We compare results obtained by different models for the stress accumulation due to rift spreading. One model that has been used to model plate boundary deformation is the so called buried dislocation model [e.g., *Árnadóttir et al.*, 2006; *LaFemina et al.*, 2005]. Such a model was used to estimate plate boundary strain in *Sigmundsson et al.* [2015]. It was also used by *Heimisson* [2015] who noted, however, that for a divergent plate boundary, a buried dislocation stress model has a minimum in tensional stress along the axis of the plate boundary and maxima on either side of the axis. For a buried dislocation at depths in the same range as the brittle-ductile boundary in Iceland, the least compressive stress becomes close to zero at the center of the rift zone at the surface. This is caused by close-to-zero gradients in the displacement field in the immediate vicinity of the plate boundary central axis (Figure C1a). Although observations, such as presented by *LaFemina et al.* [2005], cannot constrain if this change in slope occurs in nature, we nevertheless suggest that this is unlikely to be a realistic representation of the strain field. For example, in a study of the Reykjanes peninsula in SW Iceland, *Keiding et al.* [2009] considered strain rates from GPS velocities and showed that the area of highest tensional strain accumulation lies mostly in a single belt along the plate boundary. This contradicts the strain field predicted by a buried dislocation.

From the velocity profiles over the divergent plate boundaries in Iceland, such as presented by *LaFemina et al.* [2005] and *Pedersen et al.* [2009], we propose a function of the following form to describe the horizontal velocity or displacement field due to plate movements:

$$u(d) = \frac{U}{\pi} \arctan\left(\frac{d}{D}\right) \quad (13)$$

where d is the distance perpendicular to the axis of plate spreading. The value of d can be both negative and positive depending on which side of the plate boundary u is being evaluated. The surface displacement u is a vector with direction that is perpendicular to the axis of plate spreading and always pointing away from the axis. D is a free parameter that should be proportional to the locking depth and has the same unit as d . The separation of the two tectonic plates in the far field is U . Equation (13) is very similar to the screw dislocation model, which has been applied to plate boundary deformation of transform plate boundaries in Iceland and elsewhere [e.g., *Savage and Burford*, 1973; *Árnadóttir et al.*, 2006]. An equation equivalent to (13) was also proposed by *Islam and Sturkell* [2015] to fit horizontal surface velocities at the divergent plate boundary in the Eastern Volcanic Zone of Iceland. Further implementation of this model is described in Appendix C.

2.4. Probability Distribution and Path Prediction

To infer where a dike is most likely to propagate, we carry out multiple simulations of the preferred path of propagation while varying the stress model input parameters.

The simulation process goes as follows (Figure 2):

1. Stress model parameters are randomly sampled from a uniform distribution within plausible ranges.
2. The starting point of the first vertical dike segment is located at predetermined x - y coordinates. We assume all segments are 2 km long.
3. The dike segment is rotated around its starting point, and a strike is picked randomly based on a probability distribution that strongly favors strikes close to the value that minimizes the potential energy (see section 2.5).
4. Another segment is added to the end of the previous one and again the most favorable strike is found. This process is repeated for a fixed number of times.
5. Steps 1 to 4 are repeated to generate multiple simulations.

We randomly sample the parameters of the stress model from within a plausible range at the start of each simulation. For the Bárðarbunga dikes, we assume the far-field separation of the tectonic plates, or the opening

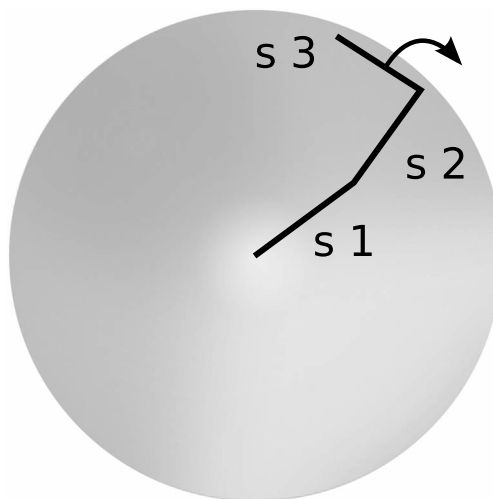


Figure 2. Schematic figure of the dike emplacement process in each simulation. Segments 1 and 2 have already been emplaced, here under a simple cone-shaped volcano, with orientation minimizing the potential energy. Segment 3 is being rotated around the end point of segment 2 to determine the most favorable orientation. This process is then repeated for the next segment.

below locking depth, U in equation (13), varies from 1.0 m to 4.2 m. This roughly corresponds to the buildup of tectonic stresses in Iceland for 50 to 220 years of plate motion. From seismic monitoring in Iceland, we infer that in the years prior to the 2014 Bárðarbunga event no dike has propagated in the same direction. A fissure eruption fed by the Bárðarbunga system is inferred to have occurred between 1794 and 1864 [Hartley and Thordarson, 2013]. The 2014–2015 eruption reactivated the same craters as this previous eruption. It is thus likely that a similar diking event caused that eruption. The location of the center axis of the rift zone is through the center of the Askja volcanic system, which geodetic measurements have suggested to be the center of the plate boundary in that region of Iceland [Sturkell and Sigmundsson, 2000]. We vary this location by ± 2.5 km in easting to estimate the error in the actual location of the plate boundary. Comparison of the average σ_3 from the slab model over 1–5 km depth range and σ_3 produced by the arctangent function revealed

the optimal range for D in equation (13) to be 4.6 km to 7.8 km. This range provides the best stress estimate for a slab of 6–8 km thickness, which is the suggested depth of the brittle-ductile boundary. The strike of the center axis of the rift is varied from E13.30°N to E15.85°N. We estimate these values by considering what three different commonly used plate motion models (NUVEL 1A [DeMets et al., 1994], MORVEL [DeMets et al., 2010], and REVEL [Sella et al., 2002]) predict for the strike of the plate motion vector of the Eurasian plate with respect to the North American plate at the north and south ends of the Bárðarbunga 2014 dike. The largest difference in the angle is between NUVEL 1A, predicting 105.85° at the northern end, and REVEL, which predicts 103.30° at the southern end. The rift axis should be perpendicular to that vector. These ranges for the parameters are summarized in Table 1. The step size in the simulations is 2 km; considering a smaller step size is not reasonable because the bedrock topography has a 0.5 km posting, and any interpolation is likely to bias the results.

The starting point of all simulations is fixed where the earthquake swarm exits the caldera for the 2014 Bárðarbunga dike. This is the beginning of the first segment identified with relative hypocenter locations presented by Sigmundsson et al. [2015]. The first segment in the simulation is forced to have strike between 97° and 157°. This is done so that the simulation starts in the direction of the propagating swarm which exited the caldera, which was 127°. We allow for a range of about $\pm 30^\circ$ to test the stability of the method. Once the first segment has been emplaced, the next one is added by searching for the most favorable orientation within $\pm 85^\circ$ of the strike of the previous segment; this allows the dike path to have a sharp turn, as was observed by Sigmundsson et al. [2015]. The orientations are evaluated in 50 equally spaced steps. We pick the most favorable strike at random but give weights to the probability of each strike based on how much it deviates from the lowest value. Our weighting discriminates strongly against values that are significantly higher than the lowest value. This is done so that some orientations that give values very close to the lowest one can also be

picked. More details follow in section 2.5.

Table 1. Randomly Sampled Stress Parameter Ranges

Parameter	Range
D equation (13)	4.55–7.80 km
U equation (13)	1.0–4.2 m
α (strike of rift axis)	13.3°–15.85°
Horizontal shift of rift axis	± 2.5 km

For implementation of the boundary element method to forecast the location of a new segment, we consider the conditions at the dike tip by superimposing stresses from the previous five segments when solving for opening and evaluating energy changes on

the segment for which the optimal strike is being determined. Perhaps a more obvious approach is to resolve for opening on all previous emplacements at each step. There is, however, a physical reason for favoring our approach over resolving for opening of all segments, as it may in reality be unlikely that energy changes in the dike, other than the tip, will influence the propagation path because instantaneous communication between the tip and other parts of the system is probably not occurring. This is discussed further in section 4.4. Our approach is also more computationally feasible since it requires considerably fewer function calls to the dislocation function, which is the most computationally expensive part of the simulations. Furthermore, considering energy changes of the whole dike results in the \mathbf{G} matrix (equation (B1)) becoming much larger than in the approach we implemented, which would slow down computation and require more memory.

We collect the locations of the start and end point of each segment of every simulation in the x - y plane and form a histogram by binning the frequency of points in a two-dimensional grid of $5 \text{ km} \times 5 \text{ km}$. We then normalize the frequency of each bin by the maximum frequency, removing bins with a value lower than 0.01 to reflect that the dike is unlikely to propagate there. In each simulation, the total dike length is 50 patches along strike, so that each simulation results in a 100 km long path prediction. This results in longer paths than observed for the Bárðarbunga dikes; however, for the hindcasting we should assume that we would not know beforehand how long the dike is going to be. The extent of the bedrock topographic map used is limited, so we remove points which fall outside this area. Because the most frequent bin is always inside that area, the relative value of the remaining bins inside the boundary is unchanged. The bedrock digital elevation model (DEM) is displayed in *Sigmundsson et al.* [2015]. The description of the bedrock DEM is given by *Björnsson and Einarsson* [1990].

2.5. Random Sampling of Strikes

When the strike that gives greatest energy release is identified, there maybe other orientations that give similar results. Even though one orientation might give a slightly lower value than another, this could, for example, be an artifact of the resolution of the bedrock topography, uncertainties in density structure, or due to numerical error. We take this into account by not always picking the strike that gave the minimum, but randomly sample with weighted probability to form a probability density function of the dike path. The weight of the i th element of the strike vector is

$$w_i = \exp \left(- \left(a \frac{\Delta U_T^i - \Delta U_T^{\min}}{\Delta U_T^{\max} - \Delta U_T^{\min}} \right)^2 \right) \quad (14)$$

where ΔU_T^i is the total energy change for the i th element of the strike vector, ΔU_T^{\min} is the energy change for the strike that minimizes the total potential energy, ΔU_T^{\max} is the energy change which maximizes the total potential energy and a is a constant. The higher the value of a , the more likely it is that the strike with lowest potential is picked. When $\Delta U_T^i = \Delta U_T^{\min}$, then $w_i = 1$; however, when $\Delta U_T^i = \Delta U_T^{\max}$, then $w_i = e^{-a^2}$. We set $a = 6$. This means that when the ratio $(\Delta U_T^i - \Delta U_T^{\min}) / (\Delta U_T^{\max} - \Delta U_T^{\min}) = 1/4$, then $w_i \approx 0.1$. The quadrant of the strike values that give the lowest potential energy values will thus have significant chances of being picked, whereas other strikes have very little chance of being picked.

3. Results

3.1. Cone-Shaped Topography

We compare the model predictions based on our approach to the classical case of a dike propagating laterally away from a cone-shaped volcano. We assume an isotropic deviatoric stress field and that the topography only induces pressure variations that are equal to the topographic load. Figure 3 shows the results for a cone with elevation of 1000 m and radius of 10 km which is exposed to 1 MPa of tensional stress along the y axis.

Both the LNB model and fixed depth model predict curved dikes that do not align perpendicular to the regional stress field under the volcanic edifice, even without the assumption of local deviatoric stress field. Assuming that the dike propagates at fixed depth makes $\Delta \phi_f$ (equation (12)) irrelevant, but both depth models predict somewhat similar paths in the presence of the edifice, although including $\Delta \phi_f$ does increase the influence of the topography. This is because the gravitational energy change of the magma tends to be at a minimum where the energy change of the crust is also at a minimum, i.e., where the opening of the dike tip is the largest. In the fixed depth case, the magma pressure remains constant, but the confining pressure changes, and the dike overpressure responds in similar manner to topography as in the LNB model.

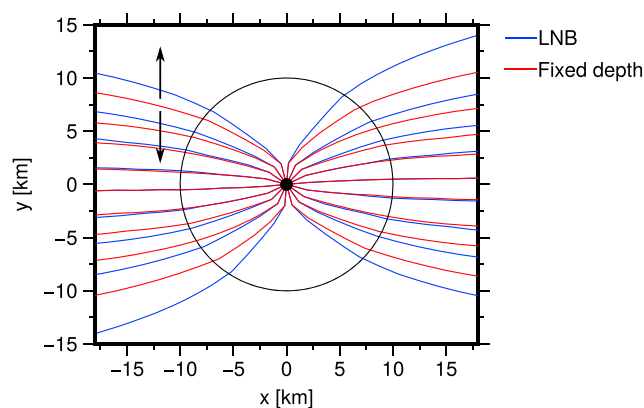


Figure 3. Predicted dike propagation paths (lines) for a cone-shaped topography. The black dot in the center is the top of a 1000 m high cone with radius of 10 km, shown as a black line. The first segment is assumed to be radial away from the top of the cone. After that the dike tip can be emplaced at any strike in the range of $\pm 85^\circ$ from the previous strike. The first radial segments are all oriented at a constant angle to each other. The imposed deviatoric stress is 1 MPa of tension in the direction of the y axis. Here we compare a LNB model with a fixed-depth model to explore the model's sensitivity to depth changes. Arrows indicate direction of tensional stress.

ing stresses, other than pressure, will eventually be, at least partially, released through faulting and fracturing. It is difficult to estimate the remaining deviatoric loading stresses in the brittle crust at time of diking. Our results suggest that topography alone, if all the deviatoric loading stresses have been released, can explain curved dikes in the vicinity of volcanic edifices. We tested running the model such that the stresses of the previous segments were not considered. In that case, the model predicted a curved path beneath the edifice, but a sudden alignment perpendicular to the regional σ_3 direction once it propagated outside the edifice. The reason the path curves outside the edifice is, therefore, due to stress field perturbations caused by the dike itself. This is equivalent to the effect where the dike alters its surrounding stress field, which was captured in the dike propagation model of Mériaux and Lister [2002].

3.2. Probability Distribution for Bárðarbunga Dikes

We compare the probability distribution from our path prediction model to the observed path of the 2014 and 1996 Bárðarbunga dikes (Figure 4). The region of high probability for the dike propagation is in a good agreement for the observed paths in 2014 and 1996, which appear to have exited the caldera in a similar location. It should be noted that the epicenter locations for the 1996 dike are less certain than for the 2014 dike.

To explore further the role of topography versus stress, we consider a few end-member cases (Figure 5) where we change the deviatoric stress or topography models, which alters pressure in the crust. When there are no stresses from plate motion considered (Figure 5a), the propagation model is only governed by pressure changes due to the topography. The path of the 2014 dike is resolved reasonably well, although the whole distribution shows considerable scatter. However, the 1996 dike and fissure extend into a low-probability area. Due to the 1996 dike being considerably shorter than that of 2014, we would expect it to be predicted with higher accuracy. The other end-member is a model purely determined by the plate boundary strain (Figure 5b), in which the topography is assumed to be flat. In that case, the model predicts propagation perpendicular to σ_3 . The 1996 dike is well constrained, but the 2014 is not hindcast. Comparison of Figures 5a and 5b suggest that the 1996 dike released deviatoric stresses in the vicinity of the exit path from the Bárðarbunga caldera, which sent the 2014 dike on a more topography-driven route. By comparing Figure 5b and Figure 4, the great importance of topography on the model becomes evident, as the influence of topography on the magma pressure is the only difference between these hindcasts.

We have so far assumed topography to only change pressure in the crust; however, in reality, loading the crust also induces deviatoric stresses. These stresses caused by buildup of topographic structures decay with time by faulting and fracturing. Figure 5c considers the end-member case where the topography is

This suggests that the $\Delta\phi_f$ term is not important to the model and that similar results can be attained without that term. We found, in a more complex simulation (section 3.2) that including that term only marginally improved the model's agreement with observations. From this we can conclude that if the dike is propagating at a fixed depth or somewhere between the LNB and a fixed depth, we can expect similar results for the forecasting model.

In a study by Roman and Jaupart [2014], they found that radial dikes which curve and eventually align to the regional stress field at Spanish Peaks, Colorado, could be explained by stress field changes induced by loading of a volcanic edifice. This could explain why these dikes are not always connected to a central magma chamber and, therefore, unlikely to be created by the rotation of a stress field due to a pressurized magma reservoir. However, load-

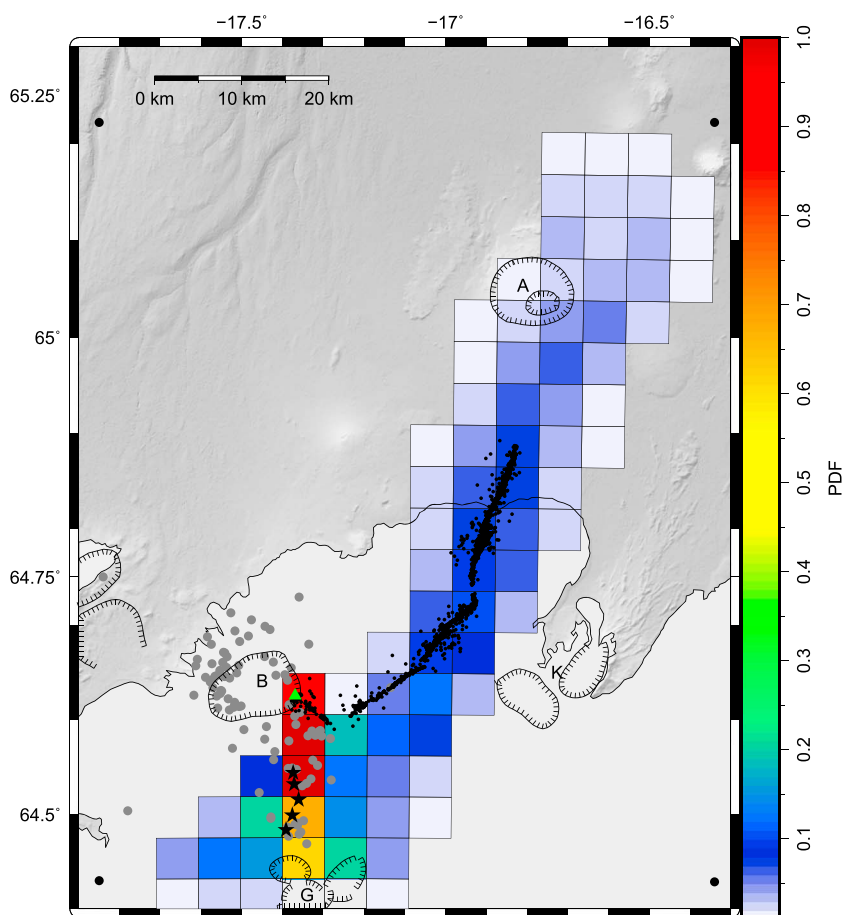


Figure 4. The dike path PDF. Small black dots are relative relocations of epicenters associated with the 2014 diking event between 16 August and 6 September [Sigmundsson *et al.*, 2015]. Larger grey dots are located events from the 1996 unrest and inferred dike propagation to the south, and the row of black stars traces the approximate location of the 1996 Gjalp eruptive fissure [Einarsson *et al.*, 1997]. The color bar shows scaled frequency, and colored square patches are top view of a 3-D histogram. The most probable location gets a value of 1 and the least probable, 0. All areas with a value less than 0.01 are removed. The green triangle is the starting point for all simulations, coinciding with the starting of the first segment identified by Sigmundsson *et al.* [2015]. Upper case A, B, G, and K indicate centers of the Askja, Bárðarbunga, Grímsvötn, and Kverkfjöll volcanoes, respectively. The four black dots are the corners of the continuous bedrock DEM used; all segments that lie outside or on this box are removed before binning to form the histogram.

acting as a load on the crust, both changing pressure and also inducing deviatoric stresses. The topographic stresses are computed by assuming all topography within a $0.5 \text{ km} \times 0.5 \text{ km}$ area and above 500 m.a.s.l. acts as a point load on a elastic half-space. The stress tensor at each point is calculated by integrating Boussinesq's equation [Boussinesq, 1885] for all point loads acting on the surface. We find that this model does not hindcast the 2014 dike. The reality is somewhere between the two end-members of all deviatoric loading stresses having been released and no deviatoric loading stresses having been released. Figures 4 and 5c display these two end-member cases. Comparison of the two suggests that the end-member where all deviatoric loading stresses have been released is a better approximation for the state of stress in the crust, at least for a very tectonically active area such as the east and north rift zones of Iceland that we are considering.

Here we have shown that the model can hindcast the paths of the 1996 and 2014 laterally propagating dikes. Moreover, we have found topography to have significant influence on the path. In spite of large uncertainty in the model of the tectonic stresses, the path is nonetheless quite well resolved. It is evident that having such a model during monitoring of the Bárðarbunga 2014 dike would have been very helpful in hazard assessment and mitigation. In Iceland, basaltic dikes are of great concern due to the relatively high likelihood of eruptions under ice, leading to explosive eruptions and catastrophic floods [Guðmundsson *et al.*, 1997]. Dikes do not form only at divergent plate boundaries, such as in Iceland or the Afar region of Ethiopia [Wright *et al.*, 2012],

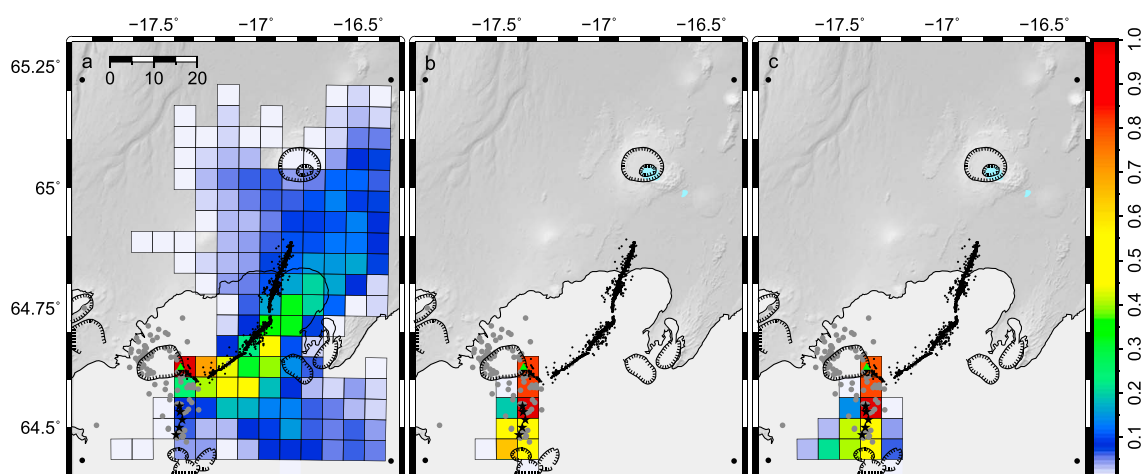


Figure 5. The same as Figure 4 except the stress model has been changed. (a) No deviatoric stress assumed in the crust. (b) All influence of topography on the model has been removed, and only the plate boundary stress model determines the path. (c) All topography above 500 m a.s.l. is assumed to be loading the crust, causing both pressure changes and deviatoric stresses.

but also in different tectonic settings. Eroded stratovolcanoes, such as the Summer Coon volcano, Colorado, demonstrate that some stratovolcanoes can produce lateral dikes in almost any direction [Poland *et al.*, 2008]. This leads to difficulty in forecasting the dike path because dikes are not restricted to well-defined zones and, therefore, of great concern in hazard mitigation. We suggest that a model such as the one presented here will help in volcanic hazard mitigation in those tectonic settings also, given an appropriate stress model. Our model, or models based on similar principles, should be used in more locations to hindcast in order to establish better its utility and limitations

4. Discussion

4.1. The Influence of Topography

Lister and Kerr [1991] argued that the dominant pressure in fracturing of the rock as a dike propagates is the dynamic pressure, i.e., the pressure that results from the fluid velocity. In the modeling presented in this study, only static pressure is assumed to influence the energy release of the dike and determine its path. We tested running the model with the dike tip always at constant overpressure, i.e., $\Delta P = \text{constant}$ as opposed to being a function of fluid and confining pressures (equation (7)), thereby mimicking a certain pressure threshold, such as induced by dynamic pressure, that is required to cause the fracture to propagate. Even for a wide range of overpressure values, the simulations were very unrealistic. At lower overpressure values (1–5 MPa), the dike paths were typically very erratic, for example, showing zigzag motion and very little agreement with observations. It is unclear why this is the case, but in this situation the overpressure is not proportional to σ_3 , and it might therefore be energetically more favorable to emplace the dike such the strain energy is released as shear rather than relaxation of tensional strain. At larger overpressure values of 10–50 MPa, the dike mostly went in circles, not propagating more than a few kilometres away from its starting point. This behavior stopped if the stress from previous emplacement was not included, and the dike then showed similar propagation as for lower overpressures values. The circular propagation is thus suggesting that the dike is being emplaced parallel to σ_3 , which is created by compression of the medium surrounding previous emplacements. We thus conclude that the model agrees in almost no way with observations if the overpressure is constant.

Assuming constant overpressure may be an oversimplification due to the directional properties of the dynamic pressure, which may be mostly responsible for the fluid fracturing caused by the magma. Due to the viscous nature of the magma, a small cavity is formed in front of the propagating dike tip, whose pressure may be maintained by exsolved magmatic volatiles or inflow of host rock pore fluids [Rubin, 1993]. The force which results from the dynamic pressure is dependent on the direction of the fluid flow field. Assuming that the flow into the dike is mostly directed along strike, it will mostly contribute to lengthening the crack, thus pushing the cavity further; however, the static pressure applies force in all directions and thus deforms the crack surface once it has been formed. Perhaps the deformation of the crack surface can ultimately be responsible

for the direction changes by perturbing the stress field in front of the dike or restricting flow channels so that magma cannot flow in certain directions. These are, however, only speculations, and we conclude that more research is needed to explain this possible discrepancy.

Several studies have indicated that topography can influence dike formation. *Hjartardóttir and Einarsson* [2015] showed that fracture density in rift zones decreases greatly in the vicinity of shield volcanoes in Iceland. This indicates that such structures might act as barriers for dikes or even arrest them. *Sigmundsson et al.* [2015] found that the Bárðarbung 2014 dike halted for 4 days in a topographic low, where it met a steep topographic increase. It still inflated at the tip until it could break through the “barrier.” This furthermore suggests that dike propagation is influenced by topography. Even though our model does not say anything about the changes in propagation speed, it still predicts that the dike will, if faced with such structures, try to change direction, if possible, and the opening of the tip will correlate negatively with the elevation of the topography (see Figure 1). *Poland et al.* [2008] found radial dikes to widen with increasing distance from a central magma chamber at the eroded Summer Coon volcano. This can be explained by topographic influence and is in agreement with our model. For example, if the dike follows the LNB, the magma pressure will increase (as the dike propagates away from the volcanic edifice) which causes widening of the dike. The same can be expected for a dike that propagates at a fixed depth; however, in that case, the decrease in confining pressure as the dike reaches shallower depth will result in widening of the dike. This corresponds well with the findings of *Pollard and Muller* [1976], which suggest that the increase in lithostatic pressure or decrease in magma pressure restricts the opening of the dike. If the opening is restricted, this will influence the fluid flow, which can cause the dike to halt and allow pressure buildup. While the dike halts, a narrow dike tip may start to freeze, thus further increasing the pressure threshold required for forward propagation. During that process, new fractures might form, and the dike can find an alternative path, erupt, or eventually break through the barrier. From this, we suggest that topographic lows are plausible eruption sites for laterally propagating dikes, as has been previously suggested [*Pinel and Jaupart*, 2004]. If a dike is propagating at the LNB, pressure must build in the tip in order for the dike to move upward, promoting fractures to propagate closer to the surface. During uphill propagation, the kinetic energy of the magma is quickly turned into gravitational potential energy, which should remove the influence of dynamic pressure.

4.2. Energy Change of the Crust

It is appropriate to address a common misconception in the literature about energy change in faulting. Commonly, equation (2) is stated to describe the strain energy change associated with faulting of any kind. However, as was demonstrated by *Dahlen* [1977] as well as *Savage and Walsh* [1978], this equation accounts for the total potential energy change of the crust. In fact, it inherently accounts for the work done by body forces. *Dahlen* [1977] rigorously investigated the energy change in faulting by applying a very generalized theoretical framework. In his derivation of equation (2), he assumes slip tangential to the fault plane. At first glance, it seems that his results may not apply to dikes; however, that assumption is only required so that the equation holds where slip occurs on internal solid-fluid interfaces. Here we consider energy changes of the fluid separately, so this is not a concern in our model. *Savage and Walsh* [1978] elegantly demonstrate that this formula may be derived simply by calculating the work done by tractions when the walls of a crack are displaced. They furthermore argue that since the Earth is a closed system, the work of the traction must also account for work of body forces. Their derivation is in no way dependent on an assumption of tangential slip.

4.3. Extra Pressure

The parameter P_{ex} in equation (8) is the extra pressure to which the whole dike is exposed. This can be caused by the connection to a magma reservoir that has a certain overpressure. As was mentioned earlier, this extra pressure could roughly represent the tensile strength of the crust. It is, however, unclear what that may be. This is due to the large differences in values found for rock in laboratory settings and for inferred kilometer-scale tensile strength. Here we set the extra pressure to 0. However, we also explored how other values influenced the forecasting model. Extra pressure of less than 5 MPa did not cause significant changes in the forecast. We did, however, find that for the cone topography, higher extra pressure resulted in greater deflection of the dikes away from the x axis. A extra pressure of 5 MPa resulted in maximum shift in the y direction of about 1–1.5 km.

At 10 MPa extra pressure, the model began to behave strangely in a manner that is typically not observed in dikes. This unrealistic propagation included zigzag paths or odd curves and kinks. This is probably caused by the dike over inflating so that it is predominantly not releasing stresses but superimposing a new stress

field that becomes the primary influence in its path, compared to the external influences of plate boundary strain or topography. It is unlikely that a dike would, in reality, inflate in such a manner without propagating further or breaking the surface. Our model is therefore strongly dependent on the pressure distribution. If dikes propagated along the σ_1 principal stress trajectories, which were present in the crust before the dike propagation, this would not be the case. More sophisticated modeling of the dike tip stresses by *Mériaux and Lister* [2002] that considers the stress changes induced by the dike as it propagates, also found strong dependence between the overpressure distribution and the dike path.

After evaluating how the model reacts to different extra pressure, we decided to set it to 0 MPa. This may not be an unreasonable assumption, because the magma chamber overpressure will not typically be felt by the dike tip due to the viscous resistance to flow [*Lister and Kerr*, 1991]. This value gives a certain lower limit to the influence of topography and assures that the paths do not exhibit unrealistic propagation modes.

4.4. Energy Changes of the System

In this study, we have mostly disregarded energy considerations of the deflating magma chamber that produces the dikes or changes in a dike once it has been emplaced. The strain release of the crust surrounding this chamber and of its magma as well as the gravitational energy decrease of the crust due to its deflation is not straightforward to include in a dike propagation forecast model. This is because of the many unknown parameters that control the magnitude of these energy terms, such as the geometry of the magma chamber, degree of inflation, depth, and volume. We consider the case of a lateral dike fed from a magma chamber at the same depth level as the dike. When it deflates, the magma chamber releases energy proportional to its volumetric contraction. We can thus infer that when a segment is emplaced, the magma chamber will release the greatest energy for the segment that has the greatest volume or, in other words, the largest opening. This is also, generally, when the energy change of the crust ($\Delta\theta_c + \Delta\phi_c$) and $\Delta\phi_f$ show the greatest energy release. It may therefore be that if the energy change of the magma chamber were considered, it would promote similar propagation paths as the $\Delta\theta_c$ and $\Delta\phi_f$ terms and, therefore, predict similar paths as our propagation model.

We also ignore the changes that might occur in the dike once it has been emplaced. These changes could be taken into account by always resolving for opening of the whole dike during the emplacement of each segment. Instead of doing that we focus solely on the tip and only solve for opening of the dike tip; however, we include the stress field from the previous segments when solving for opening of the tip. This approach is significantly more computationally feasible, as was mentioned earlier. However, considering parts of the dike or the system other than the propagating tip may also be unrealistic, as it implies instantaneous communication between the propagating tip and other parts of the system. This raises a fundamental question of whether or not the geometric emplacement of the dike is determined by the energy criteria of the dike tip or of the whole system. While some studies [e.g., *Dahm*, 2000; *Maccaferri et al.*, 2011] would favor the latter perspective, other studies [*Mériaux and Lister*, 2002] suggest that the propagation is governed by stresses acting at the dike tip. It is clear that energy dissipation must occur first in the advancing region of the dike before energy changes occur in other regions of the system through material transport. This would suggest that changes that occur in the magma chamber region or parts of the dike except the very tip will not significantly affect the direction of the advancing tip. The model we have presented here agrees well with observations. This may be either because our assumption that orientation is determined by the energy criteria of the tip only is correct or simply, as was suggested in the previous paragraph, that other factors may not affect the results considerably. We suggest that a model of dike propagation based on time-dependent variational principles, rather than quasi-static ones, is needed to better understand the determining factors in dike propagation.

4.5. Propagation Depth and Dike Height

We assumed a depth range for the dike based on what was inferred from geodetic modeling. The LNB model we have considered here is a simplification. The depth and height of laterally propagating dikes is likely to be governed by multiple processes and factors that are very difficult to estimate. These include density changes, changes in material properties, previous dike emplacements, stress history, and viscoelastic relaxation. We acknowledge that our LNB model, where the dike stays at a fixed depth below the topography, is a simplification. For example, *Pinel and Jaupart* [2004] suggested that the LNB could be even deeper beneath topographic loads.

To be able to present a model that can forecast a dike propagation path based on easily observable parameters, we assume that all aforementioned processes have secondary influences on the path. Our agreement with observations strengthens this assumption. Furthermore, we show with the cone-shaped topography

that a dike propagating at fixed depth with respect to sea level gives somewhat similar prediction as the LNB dike. It is thus likely that the prediction is not very dependent on the depth model used, although this may not be the case if the topographic effects on the stress field were considered to decrease with depth.

The vertical extent of the dike is, contrary to our assumption, likely to be influenced by the magma overpressure [Lister, 1990]. We suggest that such considerations, coupled with a similar model as presented here, may be applied to identify likely eruption sites. Perhaps the first step toward such a model would be to apply simple relationships derived by Fialko and Rubin [1999] that associate dike height and overpressure. It should be noted that these relationships may be overly simplified, as they consider the dike to be two-dimensional and ignore the influence of the free surface.

4.6. Modeling Dike Arrest

As shown by Dahm [2000] and Maccaferri *et al.* [2011, 2014], estimating the arrest of a dike is possible by considering when the energy release does not exceed a specific fracture energy threshold; however, modeling a dike growing in mass, as we have done, and determining the arrest is more complicated. This is because the energy release will depend on the overpressure and how the overpressure decays with time. To model this process accurately requires consideration a coupled system of a dike and a magma chamber feeding the dike. If we were to apply the model presented here for forecasting, we would not know beforehand how the overpressure decays. It is therefore not reasonable to include such considerations of arrest for this purpose due to the extremely variable possible decay rates. It should be noted that the energy release for the crack tip in our model at most favorable strike was generally on the order of 500–1500 TJ.

5. Conclusions

We have developed a method for forecasting the path of laterally propagating dikes given the starting point of propagation. The method is computationally feasible and can be used to form a probability distribution for dike location in near-real time. We have compared our model to the propagation of the 2014 and 1996 dikes in the Bárðarbunga volcanic system and found good agreement between predicted and observed propagation.

Our results suggest that topography plays a very important role in determining the path of laterally propagating dikes. It influences the pressure changes in the dike and thus the strain energy change and the gravitational energy change of the crust that results from dike opening. It also influences the gravitational energy change of the magma, which may influence the path.

The observed paths of the 2014 and 1996 Bárðarbunga dikes can only be explained by taking into account the deviatoric stress field from plate motion and lithostatic pressure changes from topography. It should be noted that a model that only includes pressure changes from topography can explain the observed path of the 2014 reasonably well, albeit with considerable scatter. It appears that the 1996 dike was more dominated by deviatoric stress due to plate motion, while the 2014 dike was dominated by topography. We suggest that the 1996 dike released deviatoric stress in the vicinity of the caldera, and therefore, the 2014 dike was directed on a path which is better explained by topography.

We found that curved dikes around cone-shaped topography can be explained by topography alone without the assumption of a local deviatoric stress field. This agrees with the observation that radial dikes are not always connected to a central pressurized reservoir. This has been explained by rotation of deviatoric stresses due to the loading of a volcanic edifice; however, such deviatoric stresses are not permanent (they are eventually, partially, released through faulting and diking), while pressure change remains. Nevertheless, it is likely that such dikes are influenced by both local deviatoric stress and topography. We found that a model including both deviatoric stress and pressure changes from topographic loading showed significantly less agreement with observations than a model that only considers pressure changes from topography.

We found that the commonly used buried dislocation model may, at divergent plate boundaries, poorly represent the deformation and stress field. We formulated a simple stress model based on the assumption that horizontal displacements are reasonably well described by an arctangent function. We found that an arctangent function better represents the deformation and stress of a stretched elastic slab than a buried dislocation model.

We suggest that laterally propagating dikes are most likely to erupt in topographic lows. In topographic lows the magma pressure is highest and thus the dike will be more inflated. To propagate out of a low, the dike needs to inflate further, which promotes the propagation of fractures toward the surface.

Appendix A: Density Model

The height of a dike may be on the order of kilometers, as was the case at Bárðarbunga 2014. The dike is therefore likely to be exposed to significant changes in crustal density. We apply a simple correction, in which we assume that the dike propagates in crust of density ρ_2 , but above the dike the crust has density ρ_1 . Guðmundsson and Högnadóttir [2007] estimated from the work of Carlson and Herrick [1990] and Christensen and Wilkens [1982] a plausible density range for the crust in Iceland as a function of depth. We have taken these ranges and estimated average values of $\rho_1 = 2400 \text{ kg/m}^3$ and $\rho_2 = 2700 \text{ kg/m}^3$. The density of the magma was taken to be $\rho_m = 2700 \text{ kg/m}^3$, so the criteria for LNB propagation is met. We note, however, that this model for the density of the crust is a simplification, made for computational simplicity.

Most of the propagation path of the dikes were under the Vatnajökull icecap, so we need to also consider the ice thickness and density in this model. We take the ice thickness l_i and multiply with the ratio between the ice density and rock density ρ_i/ρ_t and add to the bedrock topography's elevation. Because the ice is about three times less dense than the rock, it is less important than the bedrock topography.

Appendix B: Boundary Element Crack Model

To solve for crack tip opening using the changes in traction on the crack surface, we use a boundary element method (BEM). Assuming the crack tip is composed of a finite number of rectangular dislocations, we use Okada's Green's functions [Okada, 1992] to form the matrix \mathbf{G} presented in (B1).

$$\Delta \mathbf{T} = \mathbf{G} \mathbf{B} \Rightarrow \mathbf{B} = \mathbf{G}^{-1} \Delta \mathbf{T} \tag{B1}$$

$\Delta \mathbf{T}$ is the vector of change in traction and \mathbf{B} is the vector displacement of the crack surface. Given $\Delta \mathbf{T}$, we use (B1) to solve for \mathbf{B} , which contains the strike-slip b_s^1, \dots, b_s^k , the dip-slip b_d^1, \dots, b_d^k , and opening b_o^1, \dots, b_o^k of the dislocations, respectively. $\Delta \mathbf{T}$ is given by

$$\Delta \mathbf{T} = \begin{pmatrix} -T_s^{0,1} \\ \vdots \\ -T_s^{0,k} \\ -T_d^{0,1} \\ \vdots \\ -T_d^{0,k} \\ -\Delta P^1 \\ \vdots \\ -\Delta P^k \end{pmatrix} \tag{B2}$$

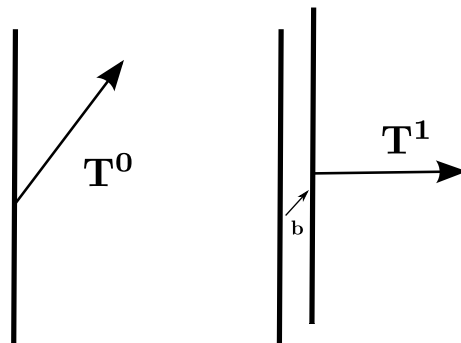


Figure B1. Figure shows a patch of area Σ^l viewed along strike, on a crack surface approximated by a single dislocation. (left) Patch before opening and (right) after opening. The traction vector before opening \mathbf{T}^0 includes a shear component. After opening, the shear is removed and the stress vector \mathbf{T}^1 is normal to the patch and equal to the magma pressure at that depth. The vector of displacement is \mathbf{b} , and its components are the opening, strike-slip, and dip-slip motion of the dislocation.

Figure B1 shows the stress vectors before and after the crack is filled with magma as well as the vector of displacement \mathbf{b} for one finite crack surface Σ^l .

\mathbf{G} has dimensions $3k \times 3k$, where k is the number of dislocations at the crack tip. Elements 1 to k of column l in \mathbf{G} are the contributions of traction in the strike direction at the center of all dislocations induced by a unit strike-slip displacement of dislocation l . Elements $k + 1$ to $2k$ are the traction in the dip direction induced by a unit strike slip in dislocation l , and elements $2k + 1$ to $3k$ in the same column are the contributions to the normal traction due to a unit strike slip on l . In the same way, column $l + k$ contains the strike, dip and normal tractions induced by a unit dip slip on l , and column $l + 2k$ the strike, dip and normal tractions induced by opening on dislocation l . This matrix is calculated for all dislocation 1 to k .

Appendix C: Arctangent Stress Model

To investigate stress field at divergent plate boundaries, we applied a finite element method (FEM) for elastostatic problems [Alberty *et al.*, 2002]. We considered a two-dimensional cross section and model the brittle crust as a rectangular slab of elastic material. The slab was assumed to extend from $x = -60$ km to $x = 60$ km, which assures that the ends extend outside the deformation zone, believed to be at least 80 km wide in North Iceland [Pedersen *et al.*, 2009]. The thickness of the slab corresponds to the depth to the brittle-ductile boundary or, equivalently, the locking depth, which has been suggested in the Askja area to be 6–8 km [Soosalu *et al.*, 2010; Key *et al.*, 2011]. A zero-traction boundary condition is applied to the top surface at $z = 0$, but the boundary condition on other surfaces is given by the displacement vector:

$$\mathbf{u} = \begin{bmatrix} \frac{U}{2} \text{sgn}(x) \\ 0 \end{bmatrix} \tag{C1}$$

where U is the far-field separation of the tectonic plate; we assume the center of the slab is at $x = 0$. Note that $\text{sgn}(x) = x/|x|$ if $x \neq 0$ and $\text{sgn}(0) = 0$ and is called the sign function.

We compare the results from the FEM modeling to our hypothesis that an arctangent function can explain the deformation at the plate boundary and from two buried dislocation models (Figure C1). One buried dislocation model consists of a single vertical tensile dislocation extending infinitely far and deep below a certain locking depth at the plate boundary axis. The other buried dislocation model consists of two infinitely long and wide horizontal faults that meet at plate boundary and slip in opposite directions, with slip vectors

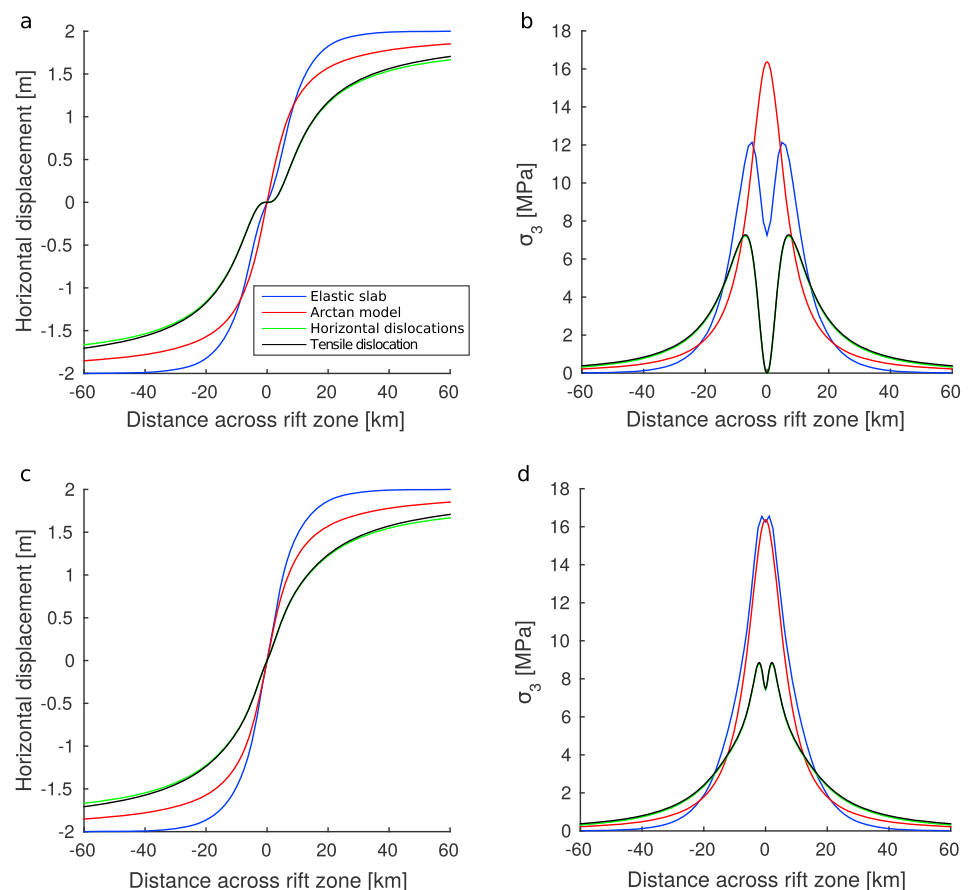


Figure C1. Comparison of deformation and stress produced by different models assuming a locking depth of 7 km for the elastic slab model and buried dislocation models and $D = 7$ km in the arctangent model. Far-field separation of the tectonic plates of 4 m is assumed in all models. Tensile stress is positive. (a) Horizontal displacements at the surface. (b) The least compressive stress at the surface. (c) Horizontal displacements at 3 km depth. (d) The least compressive stress at 3 km depth.

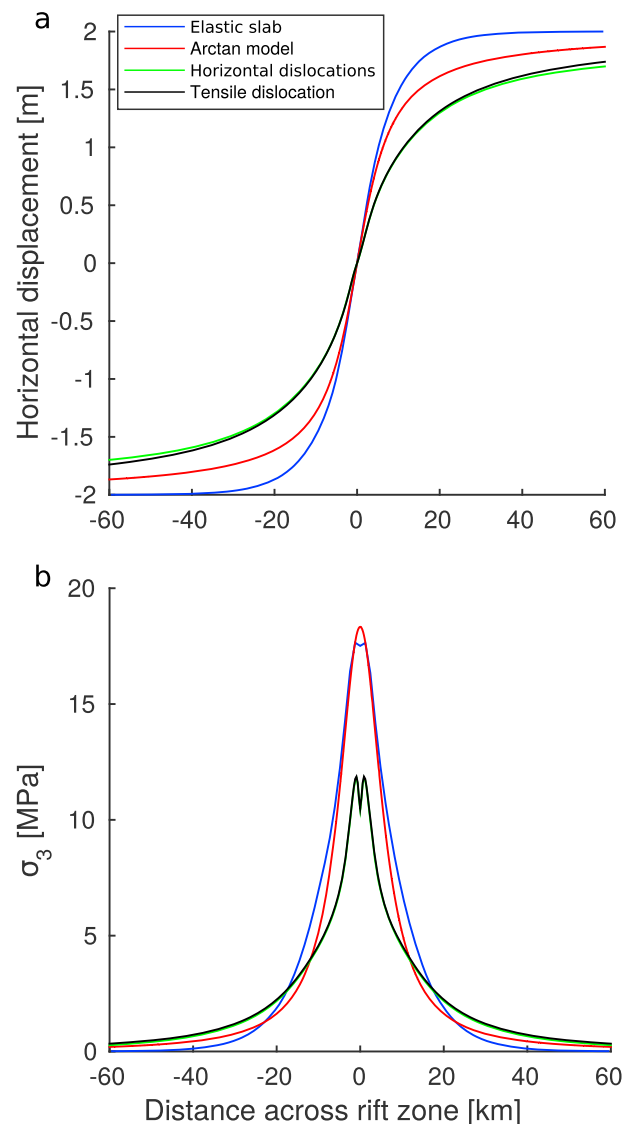


Figure C2. Comparison of average deformation and stress produced over depth range of 1–5 km by different models assuming locking depth of 7 km for the elastic slab model and dislocation models and $D = 6.25$ km in the arctangent model. Far-field separation of the tectonic plates of 4 m is assumed in all models. (a) The average horizontal displacements. (b) The average least compressive stress (tensile stress is positive).

perpendicular to the axis of plate spreading. As Figure C1 demonstrates, these two models (shown with green and black lines) create extremely similar deformation and stresses.

We conclude that the arctangent model resembles much more closely the deformation and stress of the elastic slab than the buried dislocation models. Although at the surface, the elastic slab suggests a local minimum in the least compressive stress, it is far less pronounced than for the buried dislocation models that predict zero tension in the center of the rift zone. In Figures C1b and C1c, which are calculated for 3 km depth, the arctangent and elastic slab models show very good agreement, while the buried dislocation models are significantly different.

The problem with just using the elastic slab model directly is that it is too computationally expensive, which is a problem due to the large number of simulations, where stress model parameters are varied and energy function evaluations need to be performed. By looking at the average stress over a depth range of 1–5 km, we calibrate the arctangent model using the FEM slab model and pick a value for D that best represents the average stress (Figure C2). The results are presented in Table 1.

In order to implement an arctangent model for plate boundary stress, we need a general equation for the displacement and strain. Let us assume the center axis of the plate spreading is a line with strike α east of north and that the point (x_0, y_0) is sitting on this line, where x represents easting and y northing. The slope of this line is then $a = \tan(90 - \alpha)$, and the intersection with the y axis is $b = y_0 - ax_0$

The equation of the line is

$$y = ax + b \Rightarrow y - ax - b = 0 \quad (C2)$$

The distance from this line to any point in the x - y plane is given by

$$|d(x, y)| = \frac{|y - ax - b|}{\sqrt{a^2 + 1}} \quad (C3)$$

Equation (C3) is always positive, meaning that we do not get the direction of $u(d)$ at a point $P = (x_p, y_p)$. If we drop the absolute values in equation (C3), then, if P is located under the line, d will be negative because $y_p < ax_p + b$. If P is above the line, d is positive, and if P is on the line, $d = 0$. The unit vector parallel to the line is

$$\mathbf{e}_l = \frac{1}{\sqrt{1 + b^2}} \begin{bmatrix} 1 \\ b \end{bmatrix} \quad (C4)$$

By rotating vector \mathbf{e}_l counterclockwise by 90° , using the rotation matrix \mathbf{R} , we get a new vector \mathbf{Re}_l that is parallel to the line segment between point P and the perpendicular projection of P on to the line. Let us call that point P' .

If the unit vector \mathbf{Re}_l is on the line segment PP' , it always points toward any P located above the line but away from point P located below the line. Since $u(d)$ has the same sign as d , we can have an expression for the x and y components of $u(d)$ so that the displacement vector always points away from the plate boundary:

$$\begin{bmatrix} u_x \\ u_y \end{bmatrix} = u(d)\mathbf{Re}_l \quad (C5)$$

To infer stress changes due to plate motion from the model in equation (13), we assume that the displacement field is independent of depth. The derivatives needed to calculate the strain tensor are

$$\begin{bmatrix} \frac{\partial u_x}{\partial x} \\ \frac{\partial u_x}{\partial y} \\ \frac{\partial u_y}{\partial x} \end{bmatrix} = \frac{\partial}{\partial x} u(d)\mathbf{Re}_l \quad \text{and} \quad \begin{bmatrix} \frac{\partial u_x}{\partial y} \\ \frac{\partial u_y}{\partial y} \end{bmatrix} = \frac{\partial}{\partial y} u(d)\mathbf{Re}_l \quad (C6)$$

From equation (C6), the strain and stress tensors can be calculated.

If the rift axis is oriented parallel to the y axis, then the expressions derived here are not valid because the line will not have a defined slope. Although simpler expressions can be derived for that case, one can also make use of the equations presented here by rotating the coordinate system 90° and thus assuming the rift axis is parallel to the x axis instead of the y axis.

Acknowledgments

We thank the following individuals: P. Segall whose input greatly improved this work. H. Björnsson and F. Pálsson for providing the bedrock DEM. B. Brandsdóttir for help with preparing maps and providing locations of hypocenters for the 1996 unrest. K. Vogfjörð who did the relative locations of earthquakes. P. Einarsson and S. Jónsson for helpful comments and discussion on this work. M. Poland, F. Maccaferri, and V. Pinel, whose constructive feedback significantly improved this manuscript. Some figures were produced using the GMT public domain software. The MATLAB scripts used to generate the hindcasts and path simulations is accessible by contacting the corresponding author. Support for this work was received from the European Community's Seventh Framework Programme grant 308377 (Project FUTUREVOLC).

References

- Alberty, J., C. Carstensen, S. A. Funken, and R. Klose (2002), MATLAB implementation of the finite element method in elasticity, *Computing*, 69(3), 239–263, doi:10.1007/s00607-002-1459-8.
- Anderson, E. M. (1951), *The Dynamics of Faulting and Dyke Formation With Applications to Britain*, 206 pp., Oliver and Boyd, Edinburgh.
- Árnadóttir, T., W. Jiang, K. L. Feigl, H. Geirsson, and E. Sturkell (2006), Kinematic models of plate boundary deformation in southwest Iceland derived from GPS observations, *J. Geophys. Res.*, 111, B07402, doi:10.1029/2005JB003907.
- Björnsson, H., and P. Einarsson (1990), Volcanoes beneath Vatnajökull Iceland: Evidence from radio echo-sounding, earthquakes and jökulhlaups, *Jökull*, 40, 147–168.
- Boussinesq, J. (1885), *Application des potentiels à l'étude de l'équilibre et du mouvement des solides élastiques: Principalement au calcul des déformations et des pressions que produisent, dans ces solides, des efforts quelconques exercés sur une petite partie de leur surface ou de leur intérieur: mémoire suivi de notes étendues sur divers points de physique, mathématique et d'analyse*, vol. 4, Gauthier-Villars, Paris.
- Carlson, R. L., and C. N. Herrick (1990), Densities and porosities in the oceanic crust and their variations with depth and age, *J. Geophys. Res.*, 95(B6), 9153–9170, doi:10.1029/JB095iB06p09153.
- Christensen, N. I., and R. H. Wilkens (1982), Seismic properties, density, and composition of the Icelandic crust near Reydarfjörður, *J. Geophys. Res.*, 87(B8), 6389–6395, doi:10.1029/JB087iB08p06389.
- Dahlen, F. A. (1977), The balance of energy in earthquake faulting, *Geophys. J. Int.*, 48(2), 239–261.
- Dahm, T. (2000), Numerical simulations of the propagation path and the arrest of fluid-filled fractures in the Earth, *Geophys. J. Int.*, 141(3), 623–638, doi:10.1046/j.1365-246x.2000.00102.x.
- DeMets, C., R. G. Gordon, D. F. Argus, and S. Stein (1994), Effect of recent revisions to the geomagnetic reversal time scale on estimates of current plate motions, *Geophys. Res. Lett.*, 21(20), 2191–2194, doi:10.1029/94GL02118.

- DeMets, C., R. G. Gordon, and D. F. Argus (2010), Geologically current plate motions, *Geophys. J. Int.*, *181*(1), 1–80.
- Einarsson, P., B. Brandsdóttir, M. T. Guðmundsson, H. Björnsson, K. Grönvold, and F. Sigmundsson (1997), Center of the Iceland hotspot experiences volcanic unrest, *Eos Trans. AGU*, *78*(35), 369–375, doi:10.1029/97EO00237.
- Fialko, Y. A., and A. M. Rubin (1999), What controls the along-strike slopes of volcanic rift zones?, *J. Geophys. Res.*, *104*(B9), 20,007–20,020, doi:10.1029/1999JB900143.
- Fiske, R. S., and E. D. Jackson (1972), Orientation and growth of Hawaiian volcanic rifts: The effect of regional structure and gravitational stresses, *Proc. R. Soc. A*, *329*(1578), 299–326, doi:10.1098/rspa.1972.0115.
- Guðmundsson, M. T., and T. Högnadóttir (2007), Volcanic systems and calderas in the Vatnajökull region, Central Iceland: Constraints on crustal structure from gravity data, *J. Geodyn.*, *43*(1), 153–169, doi:10.1016/j.jog.2006.09.015.
- Guðmundsson, M. T., F. Sigmundsson, and H. Björnsson (1997), Ice-volcano interaction of the 1996 Gjalp subglacial eruption, Vatnajökull, Iceland, *Nature*, *389*(6654), 954–957.
- Hartley, M. E., and T. Thordarson (2013), The 1874–1876 volcano-tectonic episode at Askja, North Iceland: Lateral flow revisited, *Geochem. Geophys. Geosyst.*, *14*, 2286–2309, doi:10.1002/ggge.20151.
- Heimisson, E. R. (2015), Lateral dike propagation forecasting model (Spálíkan fyrir kvikuganga), Master's thesis, Univ. of Iceland, Reykjavík, Iceland. [Available at <http://hdl.handle.net/1946/21719>.]
- Hjartardóttir, Á. R., and P. Einarsson (2015), The interaction of fissure swarms and monogenetic lava shields in the rift zones of Iceland, *J. Volcanol. Geotherm. Res.*, *299*, 91–102, doi:10.1016/j.jvolgeores.2015.04.001.
- Hooper, A., B. Ófeigsson, F. Sigmundsson, B. Lund, P. Einarsson, H. Geirsson, and E. Sturkell (2011), Increased capture of magma in the crust promoted by ice-cap retreat in Iceland, *Nat. Geosci.*, *4*(11), 783–786, doi:10.1038/ngeo1269.
- Islam, T., and E. Sturkell (2015), Temperature-dependent Newtonian rheology in advection-convection geodynamical model for plate spreading in Eastern Volcanic Zone, Iceland, *J. Geosci. Environ. Prot.*, *3*(5), 14–26, doi:10.4236/gep.2015.35003.
- Jónsson, S. (2012), Tensile rock mass strength estimated using InSAR, *Geophys. Res. Lett.*, *39*, L21305, doi:10.1029/2012GL053309.
- Keiding, M., B. Lund, and T. Árnadóttir (2009), Earthquakes, stress, and strain along an obliquely divergent plate boundary: Reykjanes peninsula, southwest Iceland, *J. Geophys. Res.*, *114*, B09306, doi:10.1029/2008JB006253.
- Key, J., R. S. White, H. Soosalu, and S. S. Jakobsdóttir (2011), Multiple melt injection along a spreading segment at Askja, Iceland, *Geophys. Res. Lett.*, *38*, L05301, doi:10.1029/2010GL046264.
- LaFemina, P. C., T. H. Dixon, R. Malservisi, T. Árnadóttir, E. Sturkell, F. Sigmundsson, and P. Einarsson (2005), Geodetic GPS measurements in south Iceland: Strain accumulation and partitioning in a propagating ridge system, *J. Geophys. Res.*, *110*, B11405, doi:10.1029/2005JB003675.
- Lister, J. R. (1990), Buoyancy-driven fluid fracture: Similarity solutions for the horizontal and vertical propagation of fluid-filled cracks, *J. Fluid Mech.*, *217*, 213–239, doi:10.1017/S0022112090000696.
- Lister, J. R., and R. C. Kerr (1991), Fluid-mechanical models of crack propagation and their application to magma transport in dykes, *J. Geophys. Res.*, *96*(B6), 10,049–10,077, doi:10.1029/91JB00600.
- Maccafferri, F., M. Bonafede, and E. Rivalta (2011), A quantitative study of the mechanisms governing dike propagation, dike arrest and sill formation, *J. Volcanol. Geotherm. Res.*, *208*(1–2), 39–50, doi:10.1016/j.jvolgeores.2011.09.001.
- Maccafferri, F., E. Rivalta, D. Keir, and V. Acocella (2014), Off-rift volcanism in rift zones determined by crustal unloading, *Nat. Geosci.*, *7*(4), 297–300, doi:10.1038/ngeo2110.
- Mériaux, C., and J. R. Lister (2002), Calculation of dike trajectories from volcanic centers, *J. Geophys. Res.*, *107*(B4), 2077, doi:10.1029/2001JB000436.
- Okada, Y. (1992), Internal deformation due to shear and tensile faults in a half-space, *Bull. Seismol. Soc. Am.*, *82*(2), 1018–1040.
- Pedersen, R., F. Sigmundsson, and T. Masterlark (2009), Rheologic controls on inter-rifting deformation of the Northern Volcanic Zone, Iceland, *Earth Planet. Sci. Lett.*, *281*(1–2), 14–26, doi:10.1016/j.epsl.2009.02.003.
- Pinel, V., and C. Jaupart (2004), Magma storage and horizontal dyke injection beneath a volcanic edifice, *Earth Planet. Sci. Lett.*, *221*(1–4), 245–262, doi:10.1016/S0012-821X(04)00076-7.
- Poland, M., W. Moats, and J. Fink (2008), A model for radial dike emplacement in composite cones based on observations from Summer Coon Volcano, Colorado, USA, *Bull. Volcanol.*, *70*(7), 861–875, doi:10.1007/s00445-007-0175-9.
- Pollard, D. D., and O. H. Muller (1976), The effect of gradients in regional stress and magma pressure on the form of sheet intrusions in cross section, *J. Geophys. Res.*, *81*(5), 975–984, doi:10.1029/JB081i005p00975.
- Reddy, J. N. (2013), *An Introduction to Continuum Mechanics*, Cambridge Univ. Press, New York.
- Rivalta, E., B. Taisne, A. Bungler, and R. Katz (2015), A review of mechanical models of dike propagation: Schools of thought, results and future directions, *Tectonophysics*, *638*, 1–42, doi:10.1016/j.tecto.2014.10.003.
- Roman, A., and C. Jaupart (2014), The impact of a volcanic edifice on intrusive and eruptive activity, *Earth Planet. Sci. Lett.*, *408*, 1–8, doi:10.1016/j.epsl.2014.09.016.
- Rubin, A. M. (1993), Tensile fracture of rock at high confining pressure: Implications for dike propagation, *J. Geophys. Res.*, *98*(B9), 15,919–15,935, doi:10.1029/93JB01391.
- Savage, J. C., and R. O. Burford (1973), Geodetic determination of relative plate motion in central California, *J. Geophys. Res.*, *78*(5), 832–845, doi:10.1029/JB078i005p00832.
- Savage, J. C., and J. B. Walsh (1978), Gravitational energy and faulting, *Bull. Seismol. Soc. Am.*, *68*(6), 1613–1622.
- Schultz, R. (1995), Limits on strength and deformation properties of jointed basaltic rock masses, *Rock Mech. Rock Eng.*, *28*(1), 1–15, doi:10.1007/BF01024770.
- Sella, G. F., T. H. Dixon, and A. Mao (2002), Revel: A model for recent plate velocities from space Geodesy, *J. Geophys. Res.*, *107*(B4), 2081, doi:10.1029/2000JB000033.
- Sigmundsson, F., et al. (2015), Segmented lateral dyke growth in a rifting event at Bardarbunga volcanic system, Iceland, *Nature*, *517*(7533), 191–195, doi:10.1038/nature14111.
- Soosalu, H., J. Key, R. White, C. Knox, P. Einarsson, and S. S. Jakobsdóttir (2010), Lower-crustal earthquakes caused by magma movement beneath Askja volcano on the north Iceland rift, *Bull. Volcanol.*, *72*(1), 55–62, doi:10.1007/s00445-009-0297-3.
- Sturkell, E., and F. Sigmundsson (2000), Continuous deflation of the Askja caldera, Iceland, during the 1983–1998 noneruptive period, *J. Geophys. Res.*, *105*(B11), 25,671–25,684, doi:10.1029/2000JB900178.
- Watanabe, T., T. Masuyama, K. Nagaoka, and T. Tahara (2002), Analog experiments on magma-filled cracks: Competition between external stresses and internal pressure, *Earth Planets Space*, *54*(12), e1247–e1261, doi:10.1186/BF03352453.
- Wright, T. J., et al. (2012), Geophysical constraints on the dynamics of spreading centres from rifting episodes on land, *Nat. Geosci.*, *5*(4), 242–250, doi:10.1038/ngeo1428.